



Strathprints Institutional Repository

Srinil, Narakorn (2011) *Analysis and prediction of vortex-induced vibrations of variable-tension vertical risers in linearly sheared currents*. Applied Ocean Research, 33 (1). pp. 41-53. ISSN 0141-1187

Strathprints is designed to allow users to access the research output of the University of Strathclyde. Copyright © and Moral Rights for the papers on this site are retained by the individual authors and/or other copyright owners. You may not engage in further distribution of the material for any profitmaking activities or any commercial gain. You may freely distribute both the url (<http://strathprints.strath.ac.uk/>) and the content of this paper for research or study, educational, or not-for-profit purposes without prior permission or charge.

Any correspondence concerning this service should be sent to Strathprints administrator: <mailto:strathprints@strath.ac.uk>

Analysis and Prediction of Vortex-Induced Vibrations of Variable-Tension Vertical Risers in Linearly Sheared Currents

Narakorn Srinil

Department of Naval Architecture and Marine Engineering, University of Strathclyde,
Henry Dyer Building, Glasgow, G4 0LZ, Scotland, UK

Abstract

Many studies have tackled the problem of vortex-induced vibrations (VIV) of a vertical riser with a constant tension and placed in uniform currents. In this study, attention is focused on the cross-flow VIV modelling, time-domain analysis and prediction of variable-tension vertical risers in linearly sheared currents. The partial-differential equation governing the riser transverse motion is based on a flexural tensioned-beam model with typical pinned-pinned supports. The hydrodynamic excitation model describing the modulation of lift force is based on a distributed van der Pol wake oscillator whose nonlinear equation is also partial-differential due to the implementation of a diffusion term. The variation of empirical wake coefficients with system parameters and the water depth-dependent Reynolds number is introduced. Based on the assumed Fourier mode shape functions obtained by accounting for the effect of non-uniform tension, the Galerkin technique is utilized to construct a low-dimensional multi-mode model governing the coupled fluid-riser interaction system due to VIV. Numerical simulations in the case of varying sheared flow profiles are carried out to systematically evaluate riser nonlinear dynamics and highlight the influence of fluid-structure parameters along with associated VIV aspects. In particular, the effects of shear and tensioned-beam (tension versus bending) parameters are underlined. Some comparisons with published experimental results and observations are qualitatively and quantitatively discussed. Overall parametric analysis and prediction results may be worthwhile for being a new benchmark against future experimental testing and/or numerical results predicted by an alternative model and methodology.

Keywords Vortex-Induced Vibration, Marine Riser, Sheared Current, Diffusive Wake Oscillator, Fluid-Structure Interaction

1. INTRODUCTION

Offshore slender structures exposed to ocean current flows frequently experience vortex-induced vibrations (VIV) due to the space-time modulating hydrodynamics. These nonlinear sustained oscillations increase the environmental fluid loads, harshly limit the operation of structural systems and may even ultimately lead to a catastrophic fatigue failure. In the oil & gas industry where the hydrocarbon drilling exploration and floating production activities move progressively towards deepwater arenas with depths greater than 1000 m or beyond, VIV of such key structures as drilling/production risers have become the subject of increasingly intense research investigation. Nevertheless, the prediction of deepwater riser VIV is very challenging owing to the fact that the incident flows are practically non-uniform and the associated fluid-structure interaction phenomena are highly complex. These result in a nonlinear multi-degree-of-freedom coupled system which depends on several physical and mechanical parameters. While a great deal of attention has been paid to the riser VIV modelling and prediction in the literature, most of the previous studies have been devoted to a constant-tension vertical riser in uniform current. In this study, a general low-order approximate model and numerical approach is developed to account for the case of variable-tension vertical risers placed in linearly sheared currents. Apart from capturing the effect of non-uniform tension, a qualitative and quantitative understanding of the shear flow effect on riser VIV modelling and prediction is herein ascertained which is indeed interesting from both a theoretical and practical viewpoint.

One of the indispensable requirements for estimating VIV of marine risers is to have reliable empirical information based on experimental testing with flows past rigid cylinders or flexible cylindrical structures such as cables and beams. A series of measurements provide a useful basis of hydrodynamic coefficients under specific flow and cylinder circumstances which are applicable to flexible cylinders simulating marine risers undergoing VIV. In the literature, VIV of stationary/vibrating rigid and flexible cylinders have been investigated quite comprehensively with regard to the fluid flow visualizations and wake characterizations, fluid-structure interaction phenomena and associated effects of system parameters (Sarpkaya 2004; Williamson and Govardhan 2004). An account of cylinder VIV modelling and experiment studies can be found in a review paper by Gabbai and Benaroya (2005). Recently, several joint research campaigns have been established to perform the experiment tests on large-scale model risers in realistic uniform/non-uniform flows (Baarholm et al. 2006; Chaplin et al. 2005; Lie and Kaasen 2006; Marcollo and Hinwood 2006; Tognarelli et al. 2004; Trim et al. 2005; Vandiver et al. 2009). Their main objectives were to gain better insights into the multi-mode

VIV responses of long flexible cylinders under different flow conditions, to develop benchmarking data meaningful for the calibration and validation of predictive models and computer codes, and to assess the effectiveness of some VIV suppression devices such as helical strakes. Overall, these experimental investigations demonstrate a significant effect of shear in current flows.

By focusing on the lateral or cross-flow VIV of a bare vertical riser subject to a linearly sheared current (a current profile with maximum flow velocity at the water surface decreasing monotonically towards the bottom as in Fig. 1), some relevant experimental observations are summarized as follows. Based on a 3.66 m long cylinder exposed to flow, Vandiver et al. (1996) showed how a single-mode or multi-mode response occurs under different sheared flow conditions and that the occurrence of lock-in or non-lock-in depends both on the number of potentially excited modes and the shear parameter. Tognarelli et al. (2004) analyzed a 10 m long tested pipe responding in low-mode VIV and showed the validity of some common modelling assumptions providing a good qualitative description of VIV characters. In particular, they showed how a dominant cross-flow response frequency (mode) varies approximately linearly with the maximum flow velocity or vortex shedding frequency. This is in good agreement with the analysis results of Trim et al. (2005) who analyzed a 38 m long tested riser. With regard to high-mode VIV, Lie and Kaasen (2006) analyzed a 90 m long tested riser and showed several participating modes in riser responses with highly broad-banded frequency components. These features become more apparent with increasing flow speed. It was also noticed how the computed response amplitudes were quite low when compared to those performed by similar experiments (Trim et al. 2005). Based on these experimental studies, it is worth developing a theoretical model and numerical predictive tool capable of capturing the aforesaid aspects in riser VIV and investigating systematically and parametrically the influence of shear in current. These will be herein considered and discussed in detail.

The overall goal of the present work is to construct a general low-order multi-mode interaction model capable of predicting the cross-flow responses of variable-tension vertical risers subject to linearly sheared flows and to develop a systematic numerical approach to explore the associated nonlinear dynamics due to VIV as well as the influence of several system parameters. The paper is structured as follows. In Section 2, the riser and fluid excitation models are presented which comprise both partial- and ordinary-differential equation systems. In Section 3, the approach to account for the dependence of empirical coefficients on system parameters and the water depth-varying Reynolds number is explained. Numerical

simulations and parametric investigations are conducted in Section 4 which highlights various interesting VIV aspects of vertical risers in linearly sheared currents. Some comparisons of numerical and experimental results are qualitatively and quantitatively discussed to show the validity of the presented model and numerical time-domain approach. The paper ends with conclusions in Section 5.

2. VARIABLE-TENSION RISER AND FLUID EXCITATION MODELS

In a fixed Cartesian coordinate system, a model of a variable-tension vertical riser subject to linearly sheared current is displayed in Fig. 1, with a fully-submerged span length L and typical pinned-pinned supports. Owing to the inherent slenderness and flexibility of long riser with a large aspect (length-to-diameter) ratio (L/D), the riser may be treated as a flexural tensioned-beam where both bending and axial rigidities are accounted for. In this study, the equilibrium tension in the vertical riser is considered to be non-uniform or depth-dependent. This is in contrast to many of the previous numerical or CFD-based studies which avoided the complexity of variable-tension by assuming that the tension is constant, e.g., at its maximum top-tension value.

With x being an independent spatial variable and normalized with respect to D which is spatially uniform, a general function describing the time-invariant linearly sheared flow may be given by $V(x) = V_{max}(1-\beta x)$, with the shear parameter β being defined as (Vandiver 1993)

$$\beta = \frac{\Delta V}{V_{max}} \left(\frac{D}{L} \right), \quad (1)$$

where V_{max} is the maximum velocity at sea surface, being a reference value, and ΔV is the difference in velocities at both ends. In the absence of riser initial curvatures, the incoming flow Z-axis direction is arbitrary such that the cross-flow motion of riser is aligned with Y axis following the right-hand rule. The shear parameter β depends on both the aspect ratio (L/D) and shear fraction ($\Delta V/V_{max}$). As β decreases, the correlation of vortex shedding along the riser span affecting the lock-in regime is expected to increase and eventually become maximized when $\beta = 0$ in the uniform flow case.

2.1 Partial-Differential Equations

Partial-differential equations describing the riser motion and the distributed fluid excitation are presented. By considering zero displacements and curvatures at pinned-pinned supports and non-dimensionalizing all the displacement-related variables with respect to D , the partial-

differential equation governing the cross-flow motion $v(x, t)$ of a variable-tension riser reads

$$\ddot{v} + \frac{c}{m + m_a} \dot{v} + \delta v''' - \alpha (T_r(x) v')' = \frac{H_y(x, t)}{(m + m_a) D}, \quad (2)$$

where primes denote differentiation with respect to x and overdots denote differentiation with respect to t (time). The constant mechanical parameters are the viscous damping coefficient (c), $\delta = EI/(m + m_a)D^4$, $\alpha = T_R/(m + m_a)D^2$, in which m is the riser mass (including contents), m_a the potential fluid added mass ($m_a = C_A \rho A_f$), ρ the fluid density, A_f the cross-sectional area of displaced volume, C_A the added mass coefficient ($C_A \approx 1$ for a circular cylinder), T_R the maximum top tension, EI the bending stiffness, E the elastic modulus and I the area moment of inertia. The variable-tension function – normalized by T_R – is described as $T_r(x) = 1 - xDW_e/T_R$, with W_e being the riser effective weight accounting for the buoyancy force effect. The unsteady hydrodynamic lift force H_y entailing cross-flow VIV is expressed as

$$H_y(x, t) = \frac{1}{2} \rho D V^2 C_L(x, t) = \frac{1}{2} \rho D V^2 (Q - 2\gamma \dot{v}/\omega_s), \quad (3)$$

where $C_L(x, t)$ is the space-time varying lift coefficient associated with vortex shedding, γ the so-called stall parameter and ω_s the vortex-shedding frequency (rad/s). Assuming that the Strouhal number St (Sumer and Fredsoe 2006) is constant along the riser span, $\omega_s(x) = \omega_{s, \max}(1 - \beta x)$ with $\omega_{s, \max} = 2\pi St V_{\max}/D$. In Eq.(3), the final expression was introduced by Skop and Balasubramanian (1997) to account for the fluctuation of lift coefficient through the model wake variable $Q(x, t)$ and for the stall term which captures the limited response at zero structural damping. Based on numerical and experimental studies on pivoted cylinders in sheared flows by Balasubramanian et al. (2000), Q may be governed by a diffusive van der Pol wake oscillator whose nonlinear partial-differential equation reads

$$\ddot{Q} - \omega_s G (C_{L0}^2 - 4Q^2) \dot{Q} + \omega_s^2 Q - \tau \dot{Q}'' = \omega_s F \dot{v}, \quad (4)$$

where C_{L0} is a constant lift coefficient of stationary circular cylinder, F and G the empirical wake coefficients and τ the diffusion parameter, the latter being empirically given by (Balasubramanian and Skop 1996)

$$\tau = 0.013 (L/D)^2 \omega_{s, \max} \beta. \quad (5)$$

The diffusive term in Eq. (4) has been introduced in an attempt to capture the cellular vortex-shedding feature caused by sheared flow. Experiments and wake visualizations of rigid

cylinders in shear flows have evidenced that vortices may be shed in cells of constant frequency along the span (Narasimhamurthy et al. 2009; Stansby 1976). Based on the wake oscillator in Eq.(4), Balasubramanian et al. (2000) showed a good agreement between numerical and experimental results for the sheared flow over a uniform rigid cylinder. Another diffusive wake oscillator model similar to Eq. (4) has been discussed by Mathelin and Langre (2004) who analyzed a constant-tension taut cable with zero bending. In the present study, the diffusive wake oscillator is used to analyze the response of model vertical riser with uniform properties (e.g., m , D , EI) except the space-varying tension $T_r(x)$.

2.2 Coupled Fluid-Riser Interaction Model

Towards the aim of predicting cross-flow VIV of riser and associated nonlinear multi-mode dynamics due to sheared flows, an approximate coupled fluid-riser interaction model is derived. The associated time simulations are computationally efficient when compared to the finite element- or CFD-based models. To make a comparison of obtained numerical predictions with published experimental results whose post-processed values were based on a real-valued modal analysis, a standing-wave characteristic in riser VIV is herein assumed. This assumption is justified based on some recently observed VIV of full-scale drilling pipes which tend towards standing waves with increasing amplitudes (Tognarelli et al. 2008). Also, within a CFD-based framework, Lucor et al. (2001) showed that a long flexible cylinder vibrating in linearly sheared flow exhibits a standing-wave response. Nevertheless, it is worth noting that the standing-wave response model is valid for some specific VIV cases since many real risers in sheared flows exhibit a strong travelling wave behavior (Vandiver et al. 2009).

By rearranging Eqs. (2) and (4) in their first-order differential forms and assuming that the wake variable oscillates modally and concurrently with the cylinder variable, both v and Q are postulated in terms of a full eigenbasis by letting

$$\dot{v} = A \rightarrow v(x, t) = \sum_{n=1}^{\infty} \varphi_n(x) f_n(t), \quad A(x, t) = \sum_{n=1}^{\infty} \varphi_n(x) p_n(t), \quad (6)$$

$$\dot{Q} = B \rightarrow Q(x, t) = \sum_{n=1}^{\infty} \varphi_n(x) d_n(t), \quad B(x, t) = \sum_{n=1}^{\infty} \varphi_n(x) e_n(t), \quad (7)$$

where φ_n are transverse modal shape functions and ω_n the associated natural frequencies in still water for the riser. Accurate information on ω_n and φ_n is essential and these can be analytically obtained in closed-form functions if the riser tension is constant. However, for a variable-tension vertical riser with pinned-pinned supports, ω_n and φ_n are herein analytically

and numerically determined based on a Fourier sine-based series (Srinil et al. 2007) by postulating

$$\varphi_n(x) = \sum_{n=1}^{N_s} \Upsilon_n \sin\left(\frac{n\pi x D}{L}\right). \quad (8)$$

The eigenfunction coefficients (Υ_n) are determined via a Galerkin approach, depending on the number of sine functions (N_s) retained to yield a convergence solution of frequencies and mode shapes (Srinil et al. 2007). f_n and p_n in Eq. (6) are generalized displacement and velocity coordinates of the riser whereas d_n and e_n in Eq. (7) are generalized displacement and velocity coordinates of the wake, respectively. By substituting Eqs.(6)-(7) into Eqs.(2)-(4), performing the standard Galerkin procedure (Srinil and Rega 2007; Srinil et al. 2007) with zero displacements and curvatures at end boundaries, applying the orthonormalization of modes and assuming that $\omega_{s,max} \approx \omega_n$ with a vortex-shedding frequency associated with the maximum flow speed locking on to a flexible cylinder frequency (Lucor et al. 2001), a low-order multi-mode model governing the coupled riser-wake interaction reads

$$\dot{f}_n = p_n, \quad (9)$$

$$\begin{aligned} \dot{p}_n = & -2\xi_n \omega_n p_n - \omega_n^2 f_n + \mu \omega_n^2 \sum_{i=1}^{\infty} \left[\int_0^{L/D} \varphi_n(x) (1-\beta x)^2 \varphi_i(x) dx \right] d_i + \\ & - 2\mu\gamma \omega_n \sum_{i=1}^{\infty} \left[\int_0^{L/D} \varphi_n(x) (1-\beta x) \varphi_i(x) dx \right] p_i, \end{aligned} \quad (10)$$

$$\dot{d}_n = e_n, \quad (11)$$

$$\begin{aligned} \dot{e}_n = & C_{L0}^2 \omega_n \int_0^{L/D} \varphi_n(x) (1-\beta x) G(x) \varphi_n(x) dx e_n - 4\omega_n \int_0^{L/D} (1-\beta x) G(x) \varphi_n^4(x) dx e_n d_n^2 + \\ & - \omega_{s,max}^2 \int_0^{L/D} (1-\beta x)^2 \varphi_n^2(x) dx d_n + \tau \int_0^{L/D} \varphi_n(x) \varphi_n''(x) dx e_n + \omega_n \int_0^{L/D} (1-\beta x) F(x) \varphi_n^2(x) dx p_n + \\ & + \sum_{i=1, i \neq n}^{\infty} \left[C_{L0}^2 \omega_n \int_0^{L/D} \varphi_n(x) (1-\beta x) G(x) \varphi_i(x) dx e_i - \omega_{s,max}^2 \int_0^{L/D} (1-\beta x)^2 \varphi_n(x) \varphi_i(x) dx d_i + \right. \\ & \left. + \tau \int_0^{L/D} \varphi_n(x) \varphi_i''(x) dx e_i + \omega_n \int_0^{L/D} (1-\beta x) F(x) \varphi_n(x) \varphi_i(x) dx p_i \right] + \\ & - 4\omega_n \sum_{i=1, i \neq n}^{\infty} \sum_{j=1, j \neq n}^{\infty} \sum_{k=1, k \neq n}^{\infty} \int_0^{L/D} (1-\beta x) G(x) \varphi_n(x) \varphi_i(x) \varphi_j(x) \varphi_k(x) dx d_i d_j e_k. \end{aligned} \quad (12)$$

In the absence of β , τ and multi-mode interaction terms, system Eqs.(9)-(12) reduce to those given by Srinil et al. (2009) for a single-mode cross-flow VIV in uniform flow. Therein, VIV of a catenary-shaped riser were modelled and analyzed. In this study, the multi-mode interaction effect in the wake hydrodynamics as well as the tuning of vortex-shedding ($\omega_{s,max}$) and riser natural (ω_n) frequencies are accounted for during the time-domain simulations via Eq.(12). In common with much of the literature, the modal damping ratio (ξ_n) where $\xi_n = c/2(m+m_a)\omega_n$ is assumed to be equal for all eigenmodes (i.e. $\xi \approx \xi_n$). This entails a unique mass-damping or so-called Skop-Griffin parameter defined by $S_G = \xi/\mu$, in which the relevant mass ratio is $\mu = \rho D^2/8\pi^2 St^2(m+m_a)$ (Skop and Balasubramanian 1997). Apart from the given riser (ξ , L/D , EI , W_e , T_R , m , ω_n , φ_n) and fluid (ρ , m_a , $\Delta V/V_{max}$, $\omega_{s,max}$) properties, the above approximate model captures the dependence of cross-flow VIV due to sheared flow on several empirical parameters, namely C_A , $C_{L0,\gamma}$, τ , St , F and G . Due to the variation of flow velocity V and, thus, Reynolds number (i.e., $Re = VD/\nu$, where ν is the fluid kinematic viscosity) with x , the dependence of the wake coefficients (F , G) on system parameters as well as the water depth-dependent Re is discussed next, with C_A , $C_{L0,\gamma}$, τ and St parameters being kept constant.

3. VARIATION OF EMPIRICAL WAKE COEFFICIENTS

The empirical wake coefficients F and G governing the hydrodynamic excitation in Eq. (12) may be derived as functions of system parameters defining both the flow and cylinder properties from a series of experiments. In general, cross-flow VIV of spring-mounted rigid circular cylinders in uniform flows were tested, and the associated steady-state solutions of coupled linear (cylinder) and nonlinear (wake) oscillators were determined (Gabbai and Benaroya 2005). These solutions entailed a set of formulae describing a relationship of wake coefficients to the fluid-cylinder parameters and the measured responses. Following Skop and Balasubramanian (1997), F and G depend on the measured maximum amplitude per cylinder diameter (A/D) and the frequency ratio ($\omega_{s,A}/\omega_n$) with $\omega_{s,A}$ being the vortex frequency at maximum A/D . Based on the Strouhal law (Sumer and Fredsoe 2006), the frequency ratio may also be expressed as $\omega_{s,A}/\omega_n \approx U_r St$ where U_r is a so-called reduced velocity parameter defined by $U_r = 2\pi V/\omega_n D$. Thus, one may realize that F and G depend on both A/D and U_r .

3.1 Governing Formulae

For the sake of ease, some relevant formulae derived by Skop and Balasubramanian (1997) are summarized as follows. In Eq.(12), the velocity coupling (p_n) terms are dependent on F

whose expression reads

$$F = \frac{\mu(S_G + \gamma)^2}{2} (\delta_A^2 + 4) (\Psi_A - \delta_A), \quad (13)$$

whereas the wake damping terms, controlling the self-limiting response, depend on G given by

$$G = \frac{F}{2C_{L0}^2 (S_G + \gamma)} \frac{3\delta_A^2 - 4}{\delta_A (\delta_A^2 + 4)}, \quad (14)$$

in which

$$\delta_A = - \left\{ \frac{-(8X_A - 1) + \sqrt{(8X_A - 1)^2 + 48X_A(4X_A - 1)}}{6X_A} \right\}^{1/2}, \quad (15)$$

$$X_A = \left\{ \frac{(S_G + \gamma)(A/D)}{C_{L0}} \right\}^2, \quad (16)$$

$$\Psi_A = \frac{2}{\mu(S_G + \gamma)} \left[\frac{\omega_{s,A}}{\omega_n} - 1 \right]. \quad (17)$$

Above expressions depend on the empirical parameters C_{L0} , γ and St , with the latter being included in the mass ratio parameter μ . A/D and $\omega_{s,A}/\omega_n$ are described by the following S_G -based functions

$$A/D = 0.385 / \sqrt{0.12 + S_G^2}, \quad (18)$$

$$\omega_{s,A}/\omega_n = 1.216 + \frac{0.084}{(1 + 2.66S_G^2)}. \quad (19)$$

Equations (13)-(19) reveal a highly-nonlinear relationship between wake coefficients and system parameters. One may examine *a priori* the influence of individual parameter on coefficients F and G through a graphical plot as examined by Srinil et al. (2009). For instance, when decreasing μ while keeping ξ and other parameters constant, F increases whereas G decreases. In previous studies based on a single-mode cross-flow VIV (Kim and Perkins 2002; Srinil et al. 2009), F and G were kept constant when parametrically varying V ; thus, the influence of Re was neglected. To further account for the Re effect in the VIV prediction model, a recent empirical formula given by Govardhan and Williamson (2006) is considered in place of Eq. (18). The relevant equation is given by

$$A/D = (1 - 1.12\alpha^* + 0.30\alpha^{*2}) \log(0.41 Re^{0.36}), \quad (20)$$

in which α^* is the mass-damping parameter defined as $\alpha^* = (m^* + C_A)\xi$ and m^* the cylinder-to-

fluid mass ratio defined as $m^* = m/(\pi\rho D^2/4)$. These α^* and m^* are typically referred to in the literature (Williamson and Govardhan 2004) and are defined differently from S_G and μ (Skop and Balasubramanian 1997), respectively. By making use of Eq.(20), both F and G values can be recalculated when varying V (Re) as in the case of sheared flow. This is demonstrated in the following by considering two different model risers.

3.2 Application to Model Risers in Linearly Sheared Currents

Two model vertical risers tested at the MARINTEK by ExxonMobil (Tognarelli et al. 2004) and in the Delta Flume at Delft Hydraulics (Chaplin et al. 2005) are considered. For convenience, the ExxonMobil and Delta Flume risers are denoted as EM and DF risers, respectively. Their properties and given parameters are summarized in Table 1 and will be considered, unless stated otherwise, throughout this study. Note also that, in Chaplin et al. (2005), the DF riser was subject to a stepped current but it is herein considered to be subject to linearly sheared flow towards the aim of providing its new parametric VIV studies and results. From Table 1, the two risers have comparable values of aspect ratio (L/D), mass ratio (μ or m^*) and damping ratio (ξ), and are considered to be subject to the same given parameters (ρ , γ , St , C_{L0}), flow speed range (V_{max} , V_{min}) with the same shear flow profile and parameter (β). The underlying difference is due to the values of E and T_R and that the dimensionless tensioned-beam parameter (Δ), introduced by Srinil et al. (2009) with $\Delta = L\sqrt{T_R/EI}$, is used to characterize the different contribution of axial/bending rigidity between the two risers. As given in Table 1, the EM (DF) riser is dominated by bending (tension) since it has a smaller (greater) value of Δ . This Δ parameter may affect the corresponding VIV response which will be discussed in Section 4.

As mentioned earlier, both functions $F(x)$ and $G(x)$ with varying $Re(x)$ may be determined *a priori*, but this is not straightforward in a parametric study which involves varying flow profiles with many V_{max} (V_{min}) cases since the associated integrals governing overall modal interaction coefficients in Eq.(12) have to be recalculated in every case. To circumvent such a time-consuming task, $F(x)$ and $G(x)$ based on the maximum flow speed case with $V_{max} = 2.5$ m/s are evaluated and assumed in all cases. In so doing, the analysis starts by computing F and G values at 51 discrete points along the riser from $x = 0$ (top) to $x = L/D$ (481.5). For the EM (DF) riser, it is found that F is nearly constant such that $F \approx 0.32$ (0.33) whereas G varies from 1.38 (1.15) at the top to 3.06 (2.35) at the bottom. Accordingly, a curve for $G(x)$ is constructed to determine the associated continuous functions, as demonstrated in Fig. 2 for the EM riser.

By making use of polynomials with different orders, all G values are again calculated based on these functions and compared with those obtained at the same discrete points. Increasing the order of the approximate polynomials for the purpose of convergence, it is found that, for both risers, the 7th-order polynomials provide percentage differences being overall less than 1%. Therefore, while we assume a constant $F \approx 0.32$ (0.33) for the EM (DF) riser, $G(x)$ is described by a 7th-order polynomial function as follows.

For the EM riser,

$$G(x) = 6.34 \times 10^{-18} x^7 - 9.05 \times 10^{-15} x^6 + 5.17 \times 10^{-12} x^5 - 1.47 \times 10^{-9} x^4 + 2.19 \times 10^{-7} x^3 - 1.45 \times 10^{-5} x^2 + 1.20 \times 10^{-3} x + 1.38. \quad (21)$$

For the DF riser,

$$G(x) = 4.47 \times 10^{-18} x^7 - 6.17 \times 10^{-15} x^6 + 3.42 \times 10^{-12} x^5 - 9.43 \times 10^{-10} x^4 + 1.37 \times 10^{-7} x^3 - 8.59 \times 10^{-6} x^2 + 8.68 \times 10^{-4} x + 1.15. \quad (22)$$

To demonstrate the effect of the shear parameter on empirical wake coefficients, the EM riser is again considered with $V_{min} = 0.7V_{max}$ such that β becomes 0.00062. As displayed in Fig. 2, the variation of $G(x)$ with $Re(x)$ in the case of $V_{max} = 2.5$ m/s is evaluated and the 3rd-order polynomials are now found to be sufficient as the convergent functions, giving

$$G(x) = 1 \times 10^{-10} x^3 - 1 \times 10^{-7} x^2 + 3 \times 10^{-4} x + 1.38. \quad (23)$$

Overall, Eqs. (13)-(23) and Fig. 2 highlight the dependence of wake coefficients on system parameters, spatial change in flow velocity and Re . This empirical coefficient variation would play an influential role in the riser VIV prediction. In the following, the nonlinear dynamics and VIV behaviors of EM/DF risers as well as the influence of fluid-structure parameters are parametrically investigated, along with the model validation and some qualitative/quantitative comparisons with published experimental results and observations.

4. PARAMETRIC INVESTIGATIONS AND DISCUSSION

Depending on the number of modes (N) considered, the $4N$ equations based on the autonomous system, Eq.(9-12), are simultaneously solved by a numerical time integration approach based on the fourth-order Runge-Kutta scheme, a small time step-size of 0.0001 s and properly-assigned initial conditions of modal displacements and velocities. By varying the sheared flow profiles with increasing $V(x)$ while maintaining β fixed (Eq. 1), the maximum

modal (A_n/D) and superimposed (A_R/D) amplitudes per diameter of riser are evaluated. Note that the A_n/D are useful in the analysis of multi-mode contributions and determination of dominant mode(s) in VIV. On the other hand, the A_R/D are useful in evaluating actual total responses meaningful for the ensuing prediction of stress and fatigue.

In this study, A_n/D are approximated by

$$A_n / D = \left| f_{n,\max}(t) \varphi_{n,\max}(x) \right|, \quad (24)$$

where, for the n^{th} vibration mode, $f_{n,\max}$ is the maximum f_n obtained from the steady-state time history and $\varphi_{n,\max}$ is the spatially-maximum displacement of the transverse mode shape function. With $N=(N_2-N_1)+1$ where N_2 (N_1) is the highest (lowest) mode order, the displacement profiles accounting for *all* modal contributions instantaneously in space (i) and time (j) are expressed as

$$v(x_i, t_j) = \sum_{n=N_1}^{N_2} f_n(t_j) \varphi_n(x_i). \quad (25)$$

Accordingly, A_R/D are obtained based on the spatially and temporally maximum values of $|v(x_i, t_j)|$. In some cases, the root-mean-squared (RMS) amplitude at a specific riser position $A_{\text{RMS}}(x_i)/D$ and the overall spatially-maximum value $A_{\text{RMS},\max}/D$ are computed through Eq.(25).

Prior to performing the numerical integrations of Eqs.(9-12), it is necessary to validate the fundamental eigenvalue solution obtained based on the assumed Fourier sine-based series in conjunction with the Galerkin method (Srinil et al. 2007) for variable-tension vertical risers. As an example, the comparison of the lowest seven natural frequencies in still water between numerical (with $N_s=20$) and published experimental (Chaplin et al. 2005) results for the DF riser (Table 1) is shown in Table 2 with two different values of specified top tension T_R (Δ). Note that Table 2 reports frequency values in Hz whereas in the simulations units of rad/s were used. To also demonstrate the effect of tension variation on natural frequencies, the numerical results based on the variable- and constant-tension riser models are compared. For the constant-tension model, the riser tension is assumed to be equal to T_R . For the variable-tension model, depending on the riser length and effective weight, it has been found that the percent difference between the top (maximum) and bottom (minimum) tensions with respect to the former is about 10 % for the riser with $T_R = 1546$ N and 20 % for the riser with $T_R = 813$ N.

Table 2 shows that the natural frequencies increase with T_R as expected for a fixed EI . A

better quantitative agreement is found between numerical results with the variable-tension model and experimental results. The constant-tension model entails greater percentage differences of comparisons. These discrepancies would become greater when considering higher vibration modes. Hence, it is suggested making use of the variable-tension model as in the present study. A good comparison between numerical and experimental results is also found for the EM riser when comparing with the testing results given by Tognarelli et al. (2004). In the present study, the numerically obtained frequencies of the first eight modes are equal to 1.361, 2.805, 4.408, 6.232, 8.325, 10.723, 13.451 and 16.526 Hz, respectively. These values of the EM riser are greater than all of those given in Table 2 for the DF riser due to the greater contribution of bending stiffness of the former (Table 1). Overall, the eigenvalue solution is validated. Based on both Tables 1 and 2, the parametric analysis and prediction of riser VIV in sheared flows are discussed in the following.

4.1 Riser Amplitude Diagrams: Effect of Shear and Tensioned-Beam Parameters

Depending on the assigned V range and the N modes considered, the significance of multi-mode contribution and interaction in riser VIV is now highlighted through the response amplitude diagrams which plot A_n/D (Eq. 24) versus V_{max} (0.1-2.5 m/s) in the case of gradually increasing flow speed. Emphasis is also placed on evaluating the effect of shear (β) and tension-beam (Δ) parameters on riser VIV prediction. To understand the β effect, the EM riser (Table 1) is considered with $\beta = 0.0018$ ($V_{min} = 0.14V_{max}$) vs. $\beta = 0.00062$ ($V_{min} = 0.70V_{max}$). Accordingly, the functions $G(x)$ are based on Eq.(21) and (23), respectively. With regard to the Δ effect, the DF riser is considered with different Δ values (Tables 1 and 2). Because the derivation of the empirical coefficients is independent of Δ , the functions $G(x)$ based on Eq. (22) are unchanged for the DF riser. In all riser cases, numerical simulations are based on the solution accounting for the lowest nine modes.

In Fig. 3, the response results of the EM riser are displayed. It can be seen that, when comparing Fig. 3a ($\beta = 0.0018$) to 3b ($\beta = 0.00062$), the overall modal amplitudes A_n/D approximately double as β decreases or when the current becomes less sheared. This is in good qualitative agreement with recent experimental results (Tognarelli et al. 2004; Trim et al. 2005) which show how uniform flow cases (i.e. $\beta = 0$) entail greater riser response amplitudes than sheared flow cases. In Fig. 3, the β parameter also influences the modal contribution and interaction feature as well as the associated VIV excitation range, even though the considered eigenfrequencies are identical in both Figs. 3a and 3b. For instance, A_9/D are seen to be

negligible with $\beta = 0.0018$ (Fig. 3a) whereas they are excited in a high velocity range with $\beta = 0.00062$ (Fig. 3b). Nevertheless, some qualitatively similar aspects occur in the two graphs, namely the multiple peaks and overlapping of modal amplitudes (e.g., A_4/D and A_5/D) in different flow regimes. The graphs show that the lowest vibration mode provides the maximum individual response at low velocity range. Moreover, the cross-flow predominant mode tends to follow riser eigenfrequencies by consecutively switching as V_{max} increases. This is again in good qualitative agreement with experiment observation by Tognarelli et al (2004).

Next, the A_n/D results of the DF riser are shown in Fig. 4 with two different Δ being 94 ($T_R = 1546$ N) and 133 ($T_R = 3092$ N) in Fig.4a and 4b, respectively. It can be seen that, because of the change in eigenfrequencies of different Δ cases, there is a shift in the VIV excitation range of each individual mode towards higher V_{max} values as Δ (ω_n) increases. This results in a different level of modal interaction and associated A_n/D values.

To determine the maximum attainable amplitudes of riser in linear sheared flows, the A_R/D plots taking into account overall modal superimposition are now illustrated in Fig. 5 with four different $\Delta = 68, 83, 94$ and 105 . It is illustrated that the maximum A_R/D values occur at higher V_{max} as Δ increases. These are indicated by numbers (i) to (iv) associated with the cases of $\Delta = 68, 83, 94$ and 105 , respectively. This trend implies that, if one considers a higher-tension riser case (i.e. with Δ being greater than 105), the maximum A_R/D response will occur based on the current profile having a greater V_{max} than 1.5 m/s approximately. Nevertheless, in Fig. 5, the maximum values of A_R/D are about 0.35 in all Δ cases.

Overall, it is worth emphasizing that, based on a series of sheared-flow parametric studies, a gradual variation in flow speed is necessary because the existing multiple peaks as, e.g., in Fig. 3a would disappear if the velocity increment was insufficiently small. The influence of other fluid and riser parameters such as St , L/D , τ , m and ξ on the modal (A_n/D) and superimposed (A_R/D) amplitudes of riser VIV can be conveniently investigated by following the aforesaid steps of analysis and examples. To further refine numerical prediction results, a variation in $G(x)$ functions with different sheared flow profiles may be carried out.

The reduced flow velocity parameter is well-known because it has been introduced in the VIV literature to describe the VIV excitation range (Sarpkaya 2004; Williamson and Govardhan 2004). In this study, to compare different modal excitation ranges, the reduced velocity parameter is defined by $U_m = 2\pi V_{max}/\omega_n D$ based on the V_{max} and individual modal frequency of riser (ω_n). Corresponding to Figs. 3a and 3b, the plots of U_m versus A_n/D of different modes are illustrated in Fig. 6a and 6b for the EM riser with $\beta = 0.0018$ ($V_{min} =$

$0.14V_{max}$) and $\beta = 0.00062$ ($V_{min} = 0.7V_{max}$), respectively. It can be seen that the VIV excitation range of each vibration mode appears to be larger in the higher β case (Fig. 6a) than in the lower β case (Fig. 6b), though the former having smaller response amplitudes. With non-trivial response amplitudes (A_n/D), the VIV excitation occurs in the range of $4 < U_m < 13$ in Fig. 6a whereas it does in the reduced range of $4 < U_m < 10$ (first mode) or $4 < U_m < 9$ (other modes) in Fig. 6b. Tognarelli et al. (2004) assumed the VIV excitation in the range of $4 < U_m < 10$ in their VIV analysis for the same EM riser with $\beta = 0.0018$. As the flow profile becomes less sheared in Fig. 6b, all the modal amplitudes increase whereas the associated excitation ranges are reduced. These tend towards the typical VIV results of flexible cylinders in uniform flows whose amplitudes are in the range of $1 < A_n/D < 2$ and the excitations are in the approximate range of $4 < U_m < 8$, see, e.g., Fujarra et al. (2001).

4.2 Space-Time Varying Displacements with Standing/Travelling Wave Characteristics

Depending on the multi-mode contribution, interaction and superimposition of associated amplitudes (Section 4.1), the space-time varying displacement $v(x,t)$ contours of variable-tension riser in linearly sheared flows are now visualized in Fig. 7 based on Eq.(25). For illustrative purposes, the EM riser with $\beta = 0.00062$ whose A_n/D are plotted in Fig. 3b is considered with six different V_{max} cases. The new coordinate x^* is also introduced denoting how the coordinate x , which has initially been non-dimensionalized by D , is further normalized such that its maximum value – being L/D – is equal to unity. That is $x^* = (\tilde{x}/D)/(L/D) = \tilde{x}/L$ where \tilde{x} is a dimensional vertical coordinate.

With $V_{max}=1.307$ m/s, Fig. 7a shows a clear dominance of the 5th mode response associated with $A_5/D \approx 0.51$. There is a small modulation at some internal nodes (where the minima of v occur) due to the participation of the 6th mode response whose $A_6/D \approx 0.13$ being, nevertheless, about one-fourth of A_5/D . The modulation in VIV amplitudes at riser nodes as well as anti-nodes (where the maxima of v occur) becomes more pronounced as V_{max} increases, owing to the higher multi-mode contributions. This is exemplified in Fig. 7b with $V_{max}=2.107$ m/s. In this case, three riser modes are involved with competing amplitudes of $A_7/D \approx 0.36$, $A_8/D \approx 0.27$ and $A_9/D \approx 0.11$. When increasing V_{max} slightly further to 2.147 m/s, a different dynamic scenario of the three-mode interaction takes place in Fig. 7c with $A_7/D \approx 0.38$, $A_8/D \approx 0.28$ and $A_9/D \approx 0.12$. This highlights the susceptibility of space-time variation in riser VIV.

Interestingly, as $V_{max}=2.187$ m/s in Fig. 7d, the space-time varying responses resemble a hybrid standing-travelling wave pattern along the riser span-wise direction. This is in contrast

to previous V_{max} cases (Figs. 7a-7c) which clearly exhibit the standing-wave responses. Again, even though V_{max} is slightly increased and the three 7th ($A_7/D \approx 0.34$) 8th ($A_8/D \approx 0.30$) and 9th ($A_9/D \approx 0.13$) modes are still excited in Fig. 7d as in Figs. 7b and 7c, a considerably distinctive dynamic scenario arises. Other different kinds of standing and mixed standing-travelling wave characteristics based on three-mode responses are highlighted in Figs. 7e ($V_{max} = 2.227$ m/s) and 7f ($V_{max} = 2.267$ m/s), respectively. Note that the travelling wave aspect of vertical riser in linearly sheared flow has been briefly discussed by Tognarelli et al. (2004) who considered the same EM riser. They reported that the observed travelling wave behaviour might be due to a superimposition of individual standing-wave eigenmodes. This coincides with the Galerkin-based methodology implemented in this study. More recently, insights into the travelling waves on long curved risers at higher modes have been discussed by Vandiver et al. (2009) based on the field towing experimental results.

Next, it is of interest to portray a series of spatial displacement snapshots to understand how the riser vibrates from its vertical configuration and multi-modally in sheared flow. The case of $V_{max} = 2.227$ m/s is chosen since the associated amplitude contours in Fig. 7e reveal an outstanding modulation feature. Based on the competing modes with $A_7/D \approx 0.27$, $A_8/D \approx 0.28$ and $A_9/D \approx 0.15$, the spatial v profiles at 10 consecutive time instants ($t=400-490$ s) are visualized in Fig. 8. It is seen that the overall space-time varying mode shapes are asymmetrical with respect to riser middle span. These highlight the space sharing (Tognarelli et al. 2004) of different interacting symmetric (7th, 9th) and anti-symmetric (8th) modes. Based on the number of nodes and anti-nodes (or the number of curvatures) along riser, the profile patterns resemble either the 7th mode ($t = 410, 430, 470$ and 480 s), the 8th mode ($t = 420, 440, 450, 460$ and 490 s) or the 9th mode ($t = 400$ s), depending on their modal shape characteristics, relative phases and amplitudes contributions. Such switching of a predominant mode with respect to time may be characterized as the time sharing behaviour which is currently being discussed in the literature (Violette et al. 2010) based on some recent VIV experiment results (Chaplin et al. 2005).

4.3 Time Histories, Oscillating Frequencies and Lock-In Occurrence

Time histories of the coupled riser (f_n) and wake (d_n) displacement coordinates are now illustrated along with the associated evaluation of oscillating frequencies. The cases of $V_{max} = 2.147$ and 2.187 m/s which exhibit the standing-wave (Fig. 7c) and mixed standing-travelling wave (Fig. 7d) features through displacement contours are considered, and their simulation

results of three-mode (7^{th} – 9^{th}) responses (Fig. 3b) are plotted in Fig. 9 and 10, respectively. It can be seen that riser responses are steadier than wake responses, with the latter manifesting a greater amplitude modulation (e.g., d_8 vs. f_8 in Fig. 9) and a periodic beating-type behaviour (i.e., d_7 and d_8 in Fig. 10). By relying on the f_n plots, the dominant modes with comparable amplitudes are the 7^{th} and 8^{th} modes. These modes play a together role in such sheared flow profile cases. The only difference is due to the corresponding patterns of displacement contours displayed in Fig. 7c vs. 7d.

As far as the oscillating frequencies are concerned, Fig. 11 exemplifies the Fast Fourier Transform (FFT) analysis results relevant to the time series of f_7 and f_8 vs. d_7 and d_8 in Fig. 10. Based on the considered sheared flow profile with $V_{\max} = 2.187$ m/s and the observed beating in time histories, the wake FFTs are multi harmonics which contain four frequencies being equal to 10.58, 13.19, 15.81 and 18.42 Hz, respectively, in both d_7 (Fig. 11b) and d_8 (Fig. 11d) responses. Instead of the maximum frequency (18.42 Hz) which is nearly close to $\omega_{s,\max}$, (18.59 Hz) being dominant, the two middle frequencies predominate with different amplitudes, one of them locking on to the associated riser frequency in Fig. 11a or 11c. The entrained or synchronized frequencies between Fig. 11a vs. 11b (13.19 Hz) and between Fig. 11c vs. 11d (15.81 Hz) are slightly less than the still-water frequencies $\omega_7 = 13.45$ Hz and $\omega_8 = 16.53$ Hz, respectively. This highlights the effect of varying hydrodynamic added mass caused by VIV (Sarpkaya 2004; Williamson and Govardhan 2004). Thus, Fig. 11 highlights the occurrence of lock-in condition in riser VIV subject to linearly sheared flow. This justifies the model assumption of $\omega_{s,\max} \approx \omega_n$ (Section 2.2) and confirms the lock-in event observed in the literature based on experimental (Tognarelli et al. 2004; Vandiver et al. 1996) and CFD (Lucor et al. 2001) results.

4.4 Validation of Numerical Predictions with Experimental Results

Finally, it is worthwhile validating the proposed model and obtained numerical predictions with some available experimental results. With respect to the cross-flow VIV analysis of the EM riser in linearly sheared flows, the numerical-experimental comparisons within the whole V range and a specific V are made by referring to the post-processed experiment data published by Tognarelli et al. (2004) and Yang et al. (2008), respectively. Of importance from a design viewpoint, the fatigue damage index (FDI), introduced by Tognarelli et al. (2004), is evaluated. The FDI may be approximated as $\text{FDI}(x) \approx f_d[\mathcal{E}(x)]^3$, where f_d is herein considered as the natural frequency (in Hz) of a mode dominating in VIV response (observed through, e.g., Fig.

3 or 4) and ε is the micro bending strain calculated based on a RMS value of riser dynamic curvature. In fact, the estimation of fatigue damage is usually based on a ratio of the number of stress cycles incurred over those to failure. This could be computed through the S-N curve which may entail the proportionality relationship: fatigue damage $\propto f_d \sigma^3$ (Baarholm et al. 2006). Because the stress (σ) is proportional to the bending strain that can be directly measured from experiments via strain gauges, Tognarelli *et al.* (2004) have introduced FDI to simply approximate the fatigue damage with a slope of 3 from S-N curve. This is convenient in the parametric studies and further comparisons with industrial tool predictions (Yang et al. 2008). In fact, the FDI is independent of a stress concentration factor or S-N curve intercept, but providing these values would give rise to actual fatigue damage being proportional to FDI by a constant factor. A comparison of amplitudes is herein neglected since relevant experiment results may have been affected by a typical post-processing methodology via direct double integrations of strains or acceleration at discrete sensors.

In Fig. 12, the semi-log plots compare the variation of spatially-maximum values of the predicted FDI (FDI_{max}) with increasing V_{max} for the case of $\beta = 0.0018$ (Figs. 3a and 6a). By also considering a sensitivity analysis, different values of St – as well as their different wake coefficient $G(x)$ functions (see Section 3.2) – are considered. Note that $St = 0.14$ was used by Yang et al.(2008), $St = 0.21$ was reported by Tognarelli et al. (2004) whereas this study is based on the average value with $St = 0.17$ (Table 1). It can be seen that all the predicted numerical results are in good qualitative agreement with experimental results (Tognarelli et al. 2004) by providing the increasing FDI_{max} as V_{max} increases. The quantitative differences are still seen and these may result from the lack of wake oscillator's capability of fully capturing the actual sheared flow mechanisms behind the riser, the neglected influence of in-line VIV and the assumptions imposed in the modelling. Nevertheless, when comparing the predicted spatial variation of $FDI(x)$ with experimental as well as frequency-domain analysis results (Yang et al. 2008) in the case of $V_{max} = 1.38$ m/s, results in Fig. 13 show the reduced quantitative errors for this particular flow profile. Overall, Figs. 12 and 13 illustrate how the numerical predictions are more conservative than the experimental results.

5. CONCLUSIONS

A general low-order multi-mode interactive model capable of predicting cross-flow responses of variable-tension vertical risers placed in linearly sheared currents has been developed and systematically investigated. The riser transverse motion is described by a

flexural tensioned-beam model with pinned-pinned supports, whereas the hydrodynamic excitation model governing the space-time varying lift force is based on a distributed van der Pol wake oscillator with a diffusion term. A modification of empirical wake coefficients to capture their dependence on the water depth-varying Reynolds number apart from the system mass-damping parameter has been introduced. Numerical simulations in the case of varying sheared flow profiles have been carried out to evaluate the riser nonlinear dynamics and associated VIV aspects and highlight the influence of fluid-structure parameters.

Based on the two model risers given by the relevant literature, parametric analyses and prediction results highlight the significant effect of shear parameter on empirical hydrodynamic coefficients, response amplitudes, modal contributions/interactions and VIV excitation ranges. The influence of tensioned-beam (tension vs. bending) parameter is also discussed. By gradually increasing flow velocities, insights into the space-time varying displacement contours reveal the standing wave and hybrid standing-travelling wave characteristics which are both due to the instantaneous multi-mode sharing or superimposition. As a result, the asymmetric mode shapes of the vertical riser occur during VIV, with a dominant mode switching in time. The time histories exemplify the amplitude modulation features in the wake dynamics and the entrained oscillating frequencies of riser/wake demonstrate the likelihood of lock-in conditions. Overall, numerical predictions provide good qualitative agreement with some published experimental and CFD observations. Quantitative differences between numerical and experimental results are still found which give emphasis to a necessity of further enhancing the present semi-empirical modeling and approach. This could be accomplished by, e.g., implementing a coupled in-line/cross-flow VIV model, considering a more general travelling-wave or complex-mode solution, and accounting for the non-uniform properties of riser/fluid. In any case, a new series of experimental measurements of flexible cylinders in sheared or non-uniform flows are needed towards the aim of calibrating the empirical hydrodynamic coefficients as well as benchmarking against the predicted numerical outcomes.

Acknowledgement

The author is grateful to the High Performance Computing at the Faculty of Engineering, University of Strathclyde, Glasgow, UK, in facilitating a series of numerical simulations.

REFERENCES

- Baarholm, G. S., Larsen, C. M., and Lie, H. (2006). "On fatigue damage accumulation from in-line and cross-flow vortex-induced vibrations on risers." *Journal of Fluids and Structures*, 22(1), 109-127.
- Balasubramanian, S., and Skop, R. A. (1996). "A nonlinear oscillator model for vortex shedding from cylinders and cones in uniform and shear flows." *Journal of Fluids and Structures*, 10(3), 197-214.
- Balasubramanian, S., Skop, R. A., Haan, F. L., and Szewczyk, A. A. (2000). "Vortex-excited vibrations of uniform pivoted cylinders in uniform and shear flow." *Journal of Fluids and Structures*, 14(1), 65-85.
- Chaplin, J. R., Bearman, P. W., Huera Huarte, F. J., and Pattenden, R. J. (2005). "Laboratory measurements of vortex-induced vibrations of a vertical tension riser in a stepped current." *Journal of Fluids and Structures*, 21(1), 3-24.
- Fujarra, A. L. C., Pesce, C. P., Flemming, F., and Williamson, C. H. K. (2001). "Vortex-induced vibration of a flexible cantilever." *Journal of Fluids and Structures*, 15(3-4), 651-658.
- Gabbai, R. D., and Benaroya, H. (2005). "An overview of modeling and experiments of vortex-induced vibration of circular cylinders." *Journal of Sound and Vibration*, 282(3-5), 575-616.
- Govardhan, R. N., and Williamson, C. H. K. (2006). "Defining the modified Griffin plot in vortex-induced vibration: revealing the effect of Reynolds number using controlled damping." *Journal of Fluid Mechanics*, 561, 147-180.
- Kim, W. J., and Perkins, N. C. (2002). "Two-dimensional vortex-induced vibration of cable suspensions." *Journal of Fluids and Structures*, 16(2), 229-245.
- Lie, H., and Kaasen, K. E. (2006). "Modal analysis of measurements from a large-scale VIV model test of a riser in linearly sheared flow." *Journal of Fluids and Structures*, 22(4), 557-575.
- Lucor, D., Imas, L., and Karniadakis, G. E. (2001). "Vortex dislocations and force distribution of long flexible cylinders subjected to sheared flows." *Journal of Fluids and Structures*, 15(3-4), 641-650.
- Marcollo, H., and Hinwood, J. B. (2006). "On shear flow single mode lock-in with both cross-flow and in-line lock-in mechanisms." *Journal of Fluids and Structures*, 22(2), 197-211.
- Mathelin, L., and de Langre, E. (2004). "Vortex-induced vibrations and waves under shear flow with a wake oscillator model." *European Journal of Mechanics - B/Fluids*, 24(4), 478-490.
- Narasimhamurthy, V. D., Andersson, H. I., and Pettersen, B. (2009). "Cellular vortex shedding behind a tapered circular cylinder." *Physics of Fluids*, 21, 044106.
- Sarpkaya, T. (2004). "A critical review of the intrinsic nature of vortex-induced vibrations." *Journal of Fluids and Structures*, 19(4), 389-447.
- Skop, R. A., and Balasubramanian, S. (1997). "A new twist on an old model for vortex-excited vibrations." *Journal of Fluids and Structures*, 11(4), 395-412.
- Srinil, N., and Rega, G. (2007). "Two-to-one resonant multi-modal dynamics of horizontal/inclined cables. Part II: Internal resonance activation, reduced-order models and nonlinear normal modes." *Nonlinear Dynamics*, 48(3), 253-274.

- Srinil, N., Rega, G., and Chucheepsakul, S. (2007). "Two-to-one resonant multi-modal dynamics of horizontal/inclined cables. Part I: Theoretical formulation and model validation." *Nonlinear Dynamics*, 48(3), 231-252.
- Srinil, N., Wiercigroch, M., and O'Brien, P. (2009). "Reduced-order modelling of vortex-induced vibration of catenary riser." *Ocean Engineering*, 36(17-18), 1404-1414.
- Stansby, P. K. (1976). "The locking-on of vortex shedding due to cross stream vibration of circular cylinders in uniform and sheared flows." *Journal of Fluid Mechanics*, 74, 641-668.
- Sumer, B. M., and Fredsoe, J. (2006). *Hydrodynamics Around Cylindrical Structures*: World Scientific.
- Tognarelli, M. A., Slocum, S. T., Frank, W. R., and Campbell, R. B. (2004). "VIV response of a long flexible cylinder in uniform and linearly sheared currents." *Offshore Technology Conference*, OTC-16338, 1-12.
- Tognarelli, M. A., Taggart, S., and Campbell, M. (2008). "Actual VIV fatigue response of full scale drilling risers: with and without suppression devices." *Proceedings of the 27th International Conference on Offshore Mechanics and Arctic Engineering*, OMAE2008-57046, 1-13.
- Trim, A. D., Braaten, H., Lie, H., and Tognarelli, M. A. (2005). "Experimental investigation of vortex-induced vibration of long marine risers." *Journal of Fluids and Structures*, 21(3), 335-361.
- Vandiver, J. K. (1993). "Dimensionless parameters important to the prediction of vortex-induced vibration of long, flexible cylinders in ocean currents." *Journal of Fluids and Structures*, 7(5), 423-455.
- Vandiver, J. K., Allen, D., and Li, L. (1996). "The occurrence of lock-in under highly sheared conditions." *Journal of Fluids and Structures*, 10(5), 555-561.
- Vandiver, J. K., Jaiswal, V., and Jhingran, V. (2009). "Insights on vortex-induced, traveling waves on long risers." *Journal of Fluids and Structures*, 25(4), 641-653.
- Violette, R., de Langre, E., and Szydlowski, J. (2010). "A linear stability approach to vortex-induced vibrations and waves." *Journal of Fluids and Structures*, 26, 442-466.
- Williamson, C. H. K., and Govardhan, R. (2004). "Vortex-induced vibrations." *Annual Review of Fluid Mechanics*, 36, 413-455.
- Yang, G., Frank, W. R., Campbell, R. B., and Slocum, S. T. (2008). "VIV model test data comparison with Shear7 v.4.5." *Proceedings of the 27th International Conference on Offshore Mechanics and Arctic Engineering*, OMAE2008-57108, 1-12.

TABLE

- 1 Properties and input parameters of considered risers and current flows
- 2 Numerical and experimental comparisons of natural frequencies in still water (Hz) for the DF riser with two different Δ

FIGURE

- 1 A schematic model of a variable-tension vertical riser placed in linearly sheared current
- 2 Variation of wake coefficient G with non-dimensional vertical coordinate and Re for the EM riser subject to sheared flows with two different β : line with circles (solid line) denotes $\beta = 0.0018$ (0.00062)
- 3 Variation of maximum multi modal amplitudes with varying V_{max} for the EM riser with $\Delta = 22$: (a) $\beta = 0.0018$, (b) $\beta = 0.00062$
- 4 Variation of maximum multi modal amplitudes with varying V_{max} for the DF riser with $\beta = 0.0018$: (a) $\Delta = 94$, (b) $\Delta = 133$
- 5 Variation of maximum superimposed amplitudes with varying V_{max} for the DF riser with four different Δ
- 6 Variation of A_n/D with U_{rn} for the EM riser: (a) $\beta = 0.0018$, (b) $\beta = 0.00062$
- 7 Space-time varying displacement contours for the EM riser with $\beta = 0.00062$: (a) $V_{max} = 1.307$ m/s, (b) $V_{max} = 2.107$ m/s, (c) $V_{max} = 2.147$ m/s, (d) $V_{max} = 2.187$ m/s, (e) $V_{max} = 2.227$ m/s, (f) $V_{max} = 2.267$ m/s
- 8 Space-time varying displacement profiles or mode shapes at ten different snapshots for the EM riser with $\beta = 0.00062$ and $V_{max} = 2.227$ m/s
- 9 Time histories of riser (f) and wake (d) modal displacement coordinates for the EM riser with $V_{max} = 2.147$ m/s
- 10 Time histories of riser (f) and wake (d) modal displacement coordinates for the EM riser with $V_{max} = 2.187$ m/s
- 11 Oscillating frequencies of the two dominant 7th and 8th modes associated with modal time histories in Fig. 10
- 12 Comparison of numerical results with different assigned St and experimental results in terms of FDI_{max} with varying V_{max} for the EM riser with $\beta = 0.0018$
- 13 Comparison of numerical and experimental results in terms of spatial variation of FDI for the EM riser with $\beta = 0.0018$ and $V_{max} = 1.38$ m/s

Table 1

Properties and Parameters	Experimented Riser		SI Units
	ExxonMobil	Delta Flume	
L	9.63	13.12	m
D	20	28	mm
T_R	700	1546	N
E	1.025×10^{11}	1.82×10^9	N/m ²
ρ	1000	1000	kg/m ³
V_{max}	0.1-2.5	0.1-2.5	m/s
V_{min}	$0.14V_{max}$	$0.14V_{max}$	m/s
Re_{max}	3.8×10^4	5.4×10^4	-
ζ	0.003	0.0033	-
μ	0.173	0.139	-
m^*	2.23	3	-
St	0.17	0.17	-
γ	0.183	0.183	-
CL_0	0.28	0.28	-
β	0.0018	0.0018	-
Δ	22	94	-

Table 2

Mode	$T_R = 813 \text{ N}$ ($\Delta \approx 68$)			$T_R = 1546 \text{ N}$ ($\Delta \approx 94$)		
	Chaplin et al. (2005)	Variable tension model	Constant tension model	Chaplin et al. (2005)	Variable tension model	Constant tension model
1	0.633	0.657	0.693	0.899	0.930	0.955
2	1.329	1.319	1.390	1.815	1.862	1.913
3	1.954	1.990	2.095	2.741	2.802	2.877
4	2.625	2.674	2.814	3.614	3.751	3.850
5	3.312	3.377	3.550	4.561	4.712	4.836
6	4.028	4.102	4.306	5.525	5.690	5.838
7	4.753	4.853	5.088	6.439	6.687	6.858

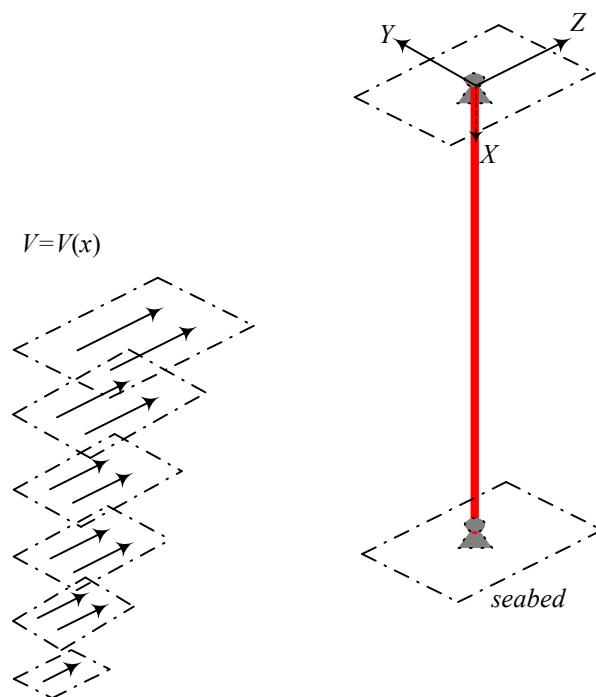


Figure 1

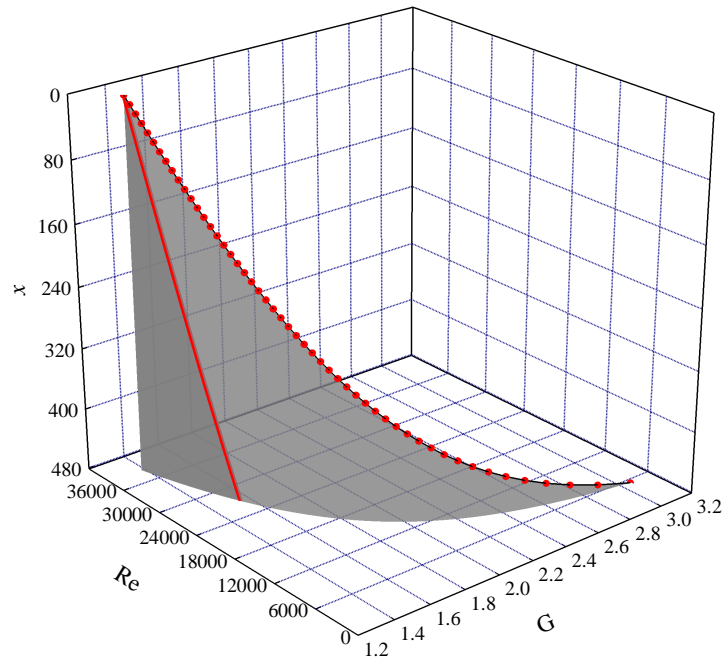


Figure 2

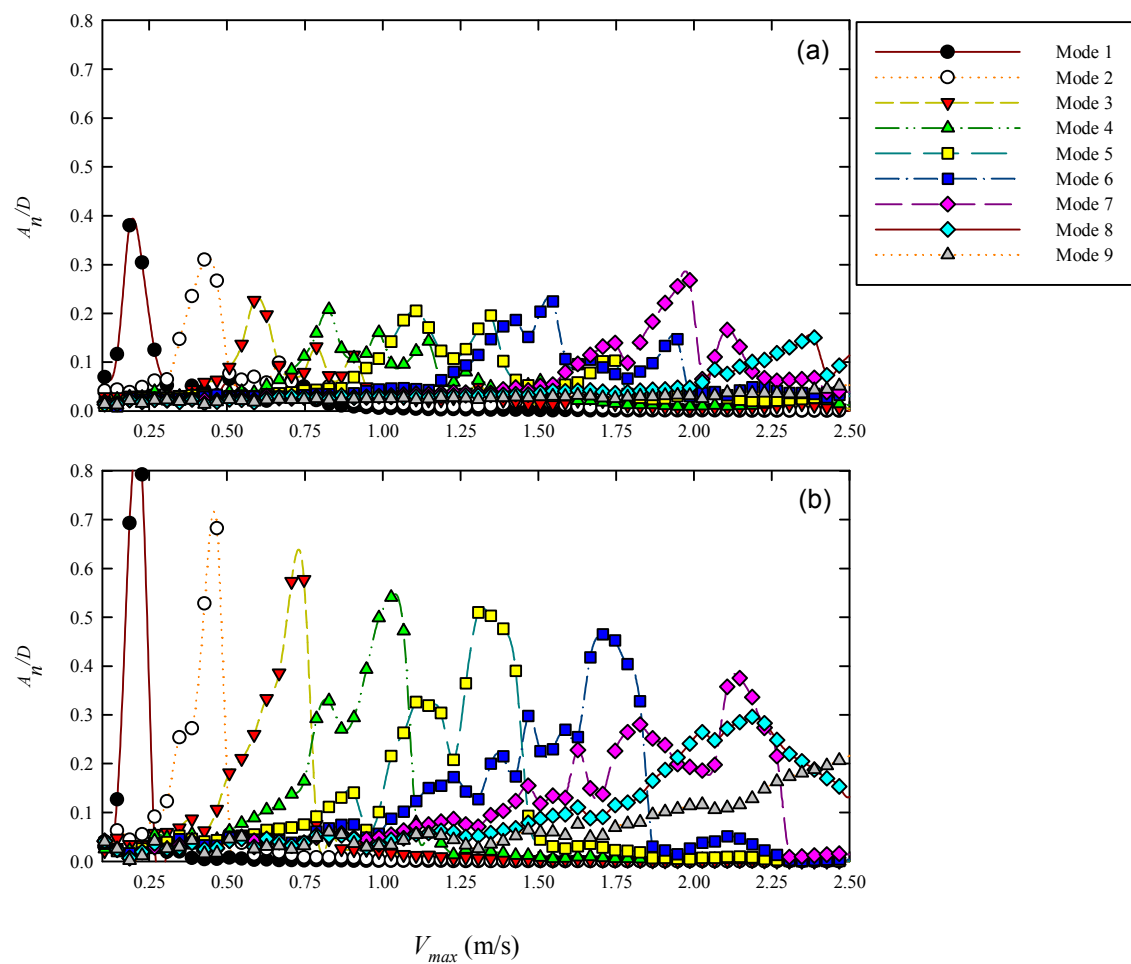


Figure 3

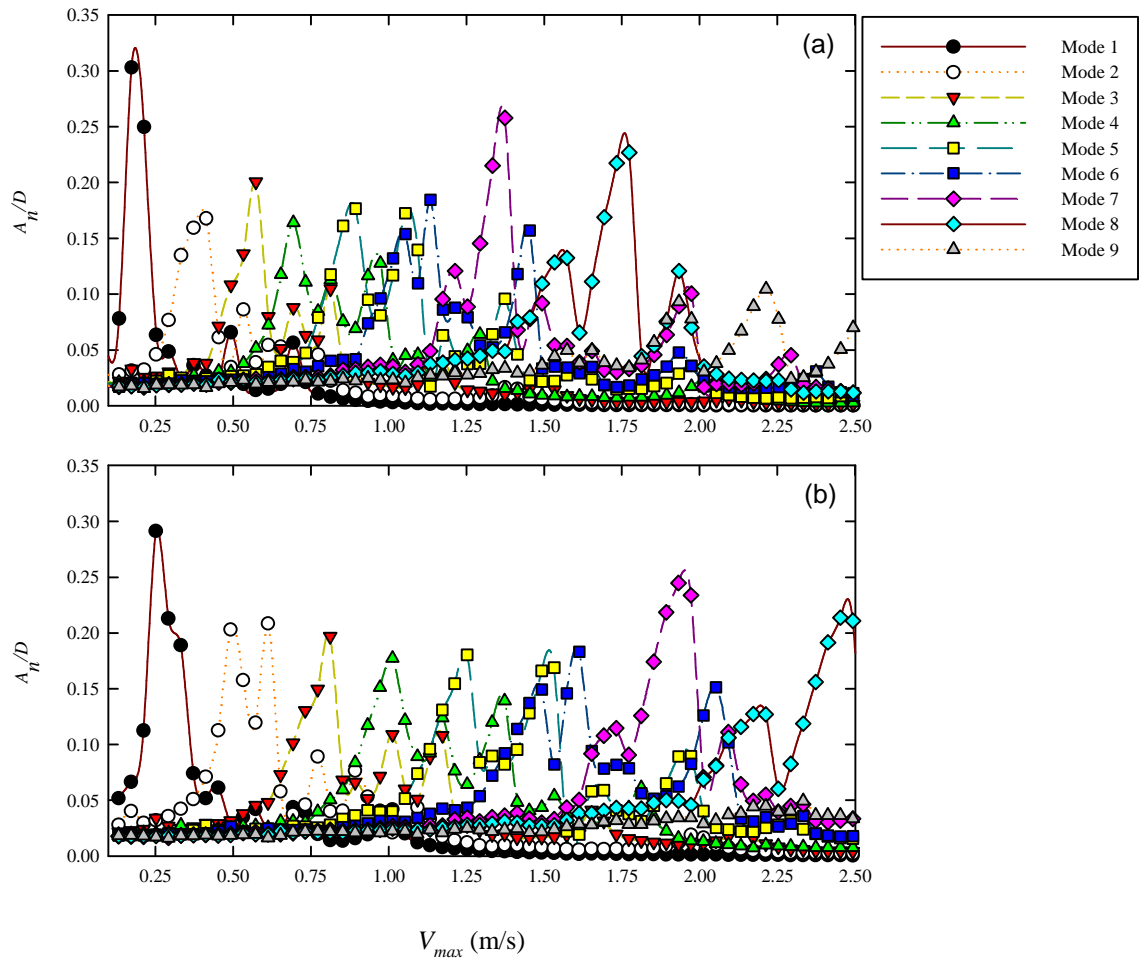


Figure 4

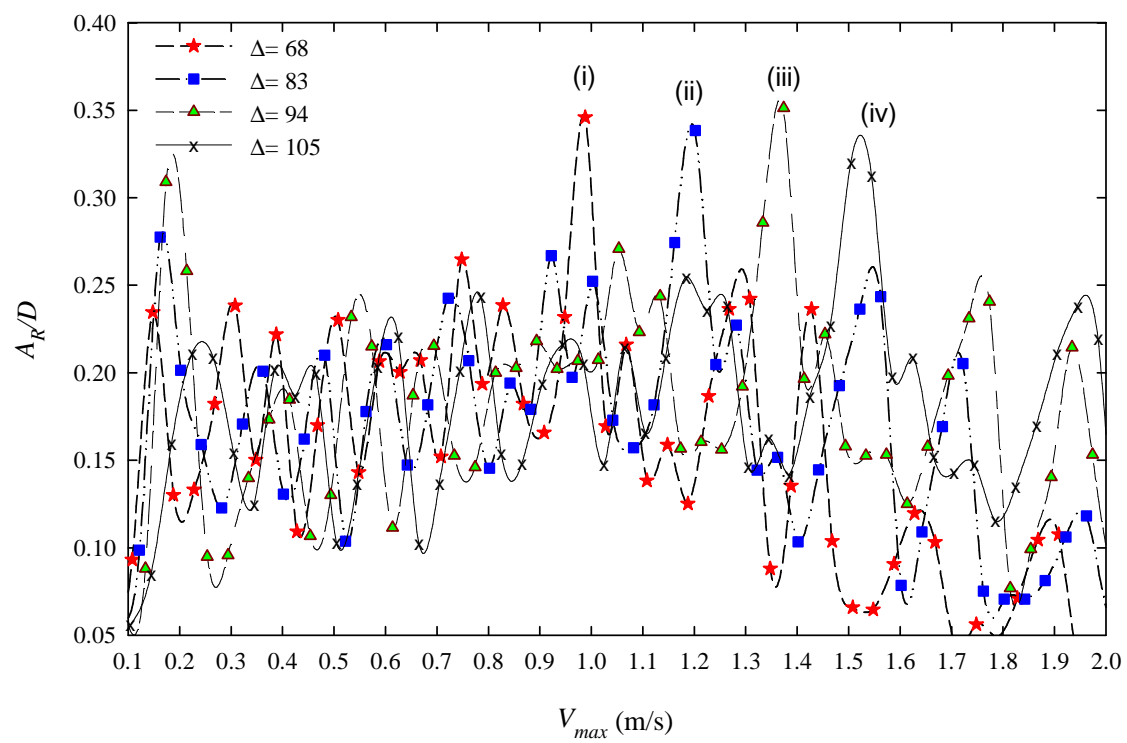


Figure 5

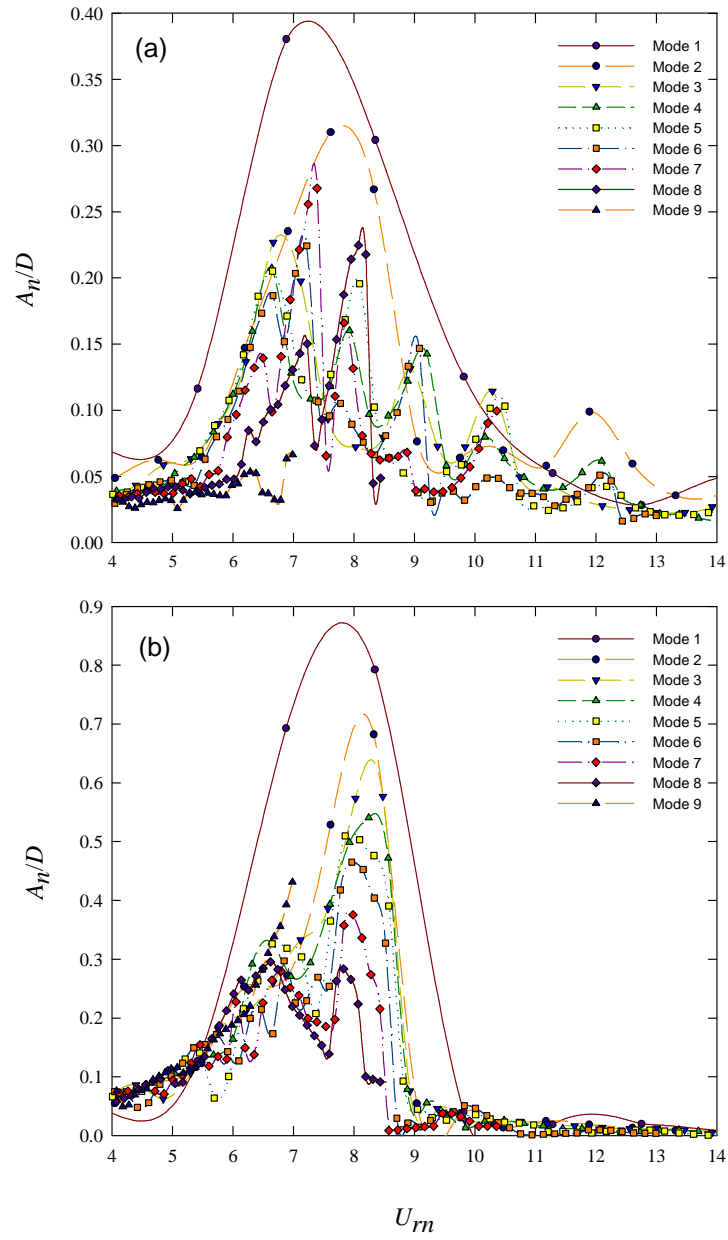


Figure 6

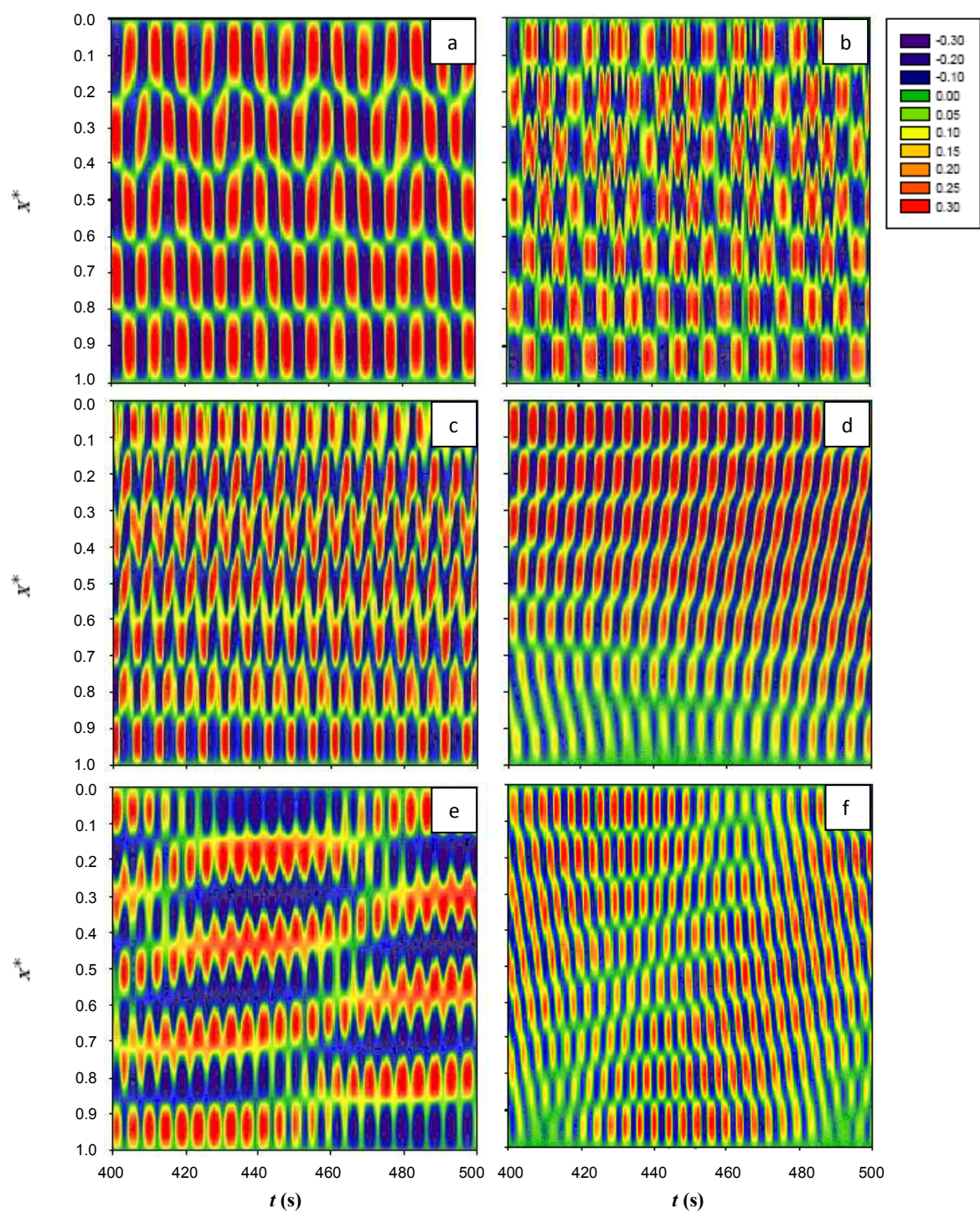


Figure 7

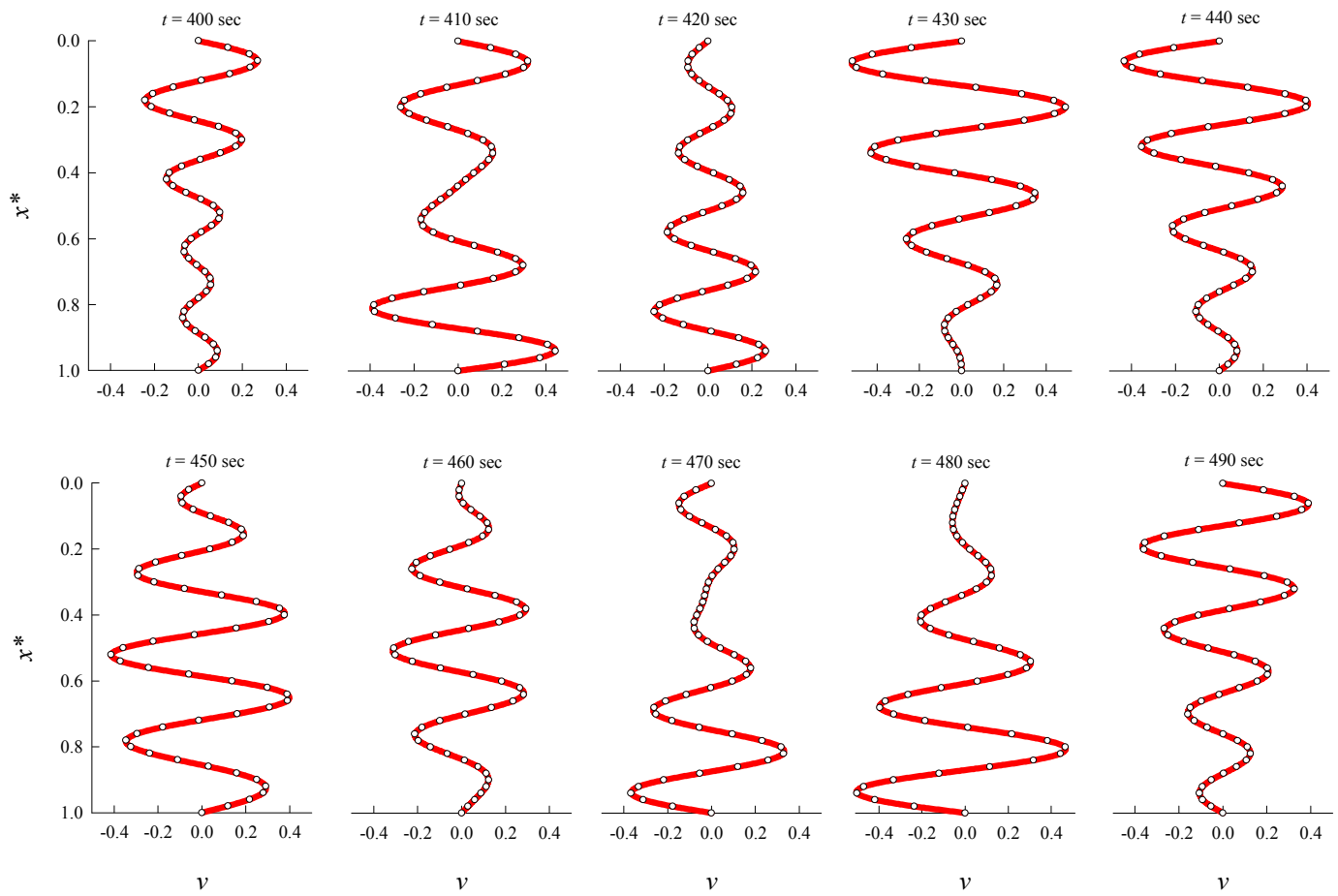


Figure 8

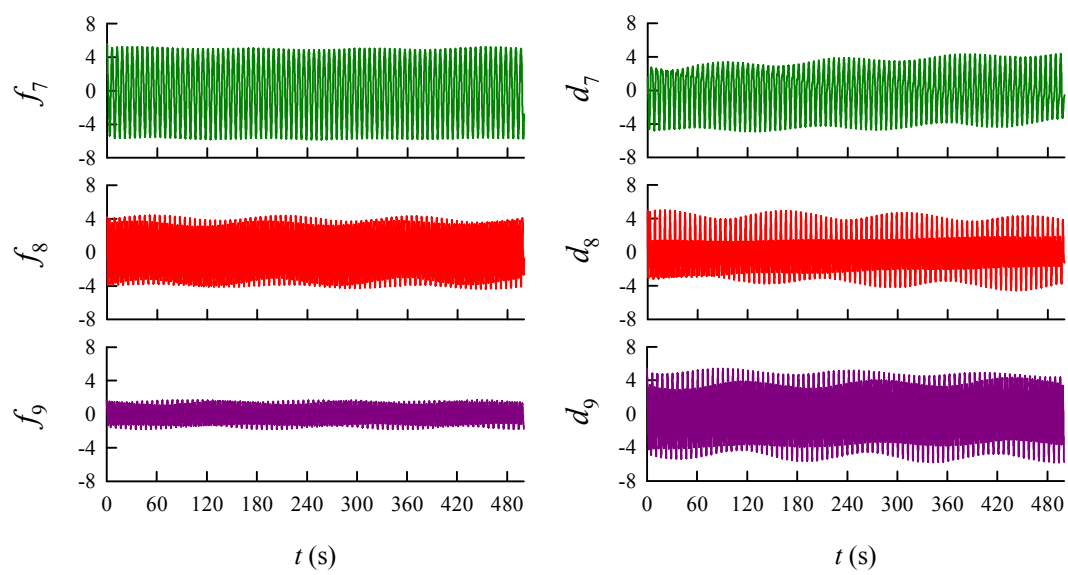


Figure 9

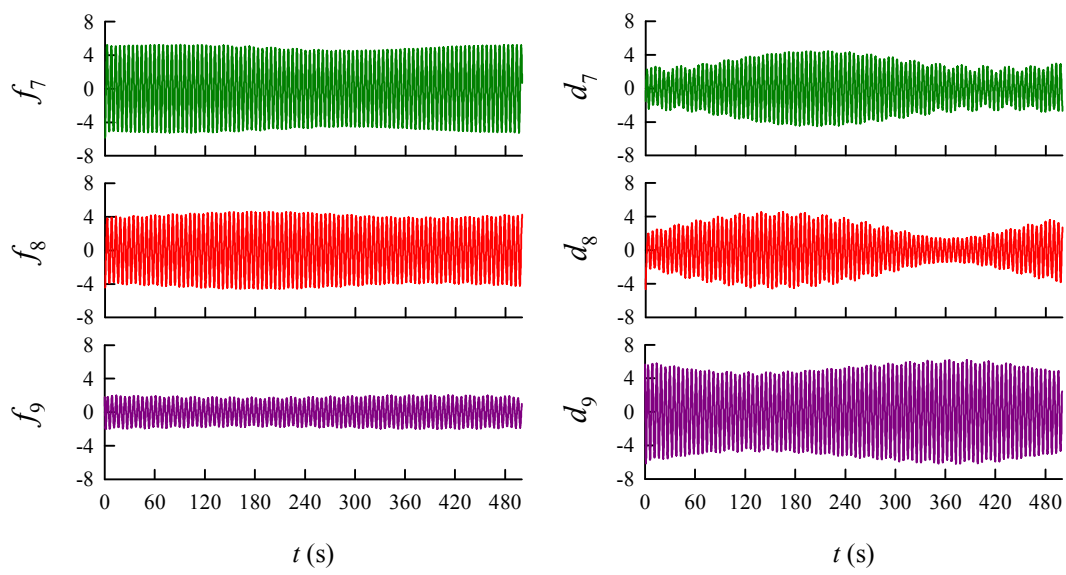


Figure 10

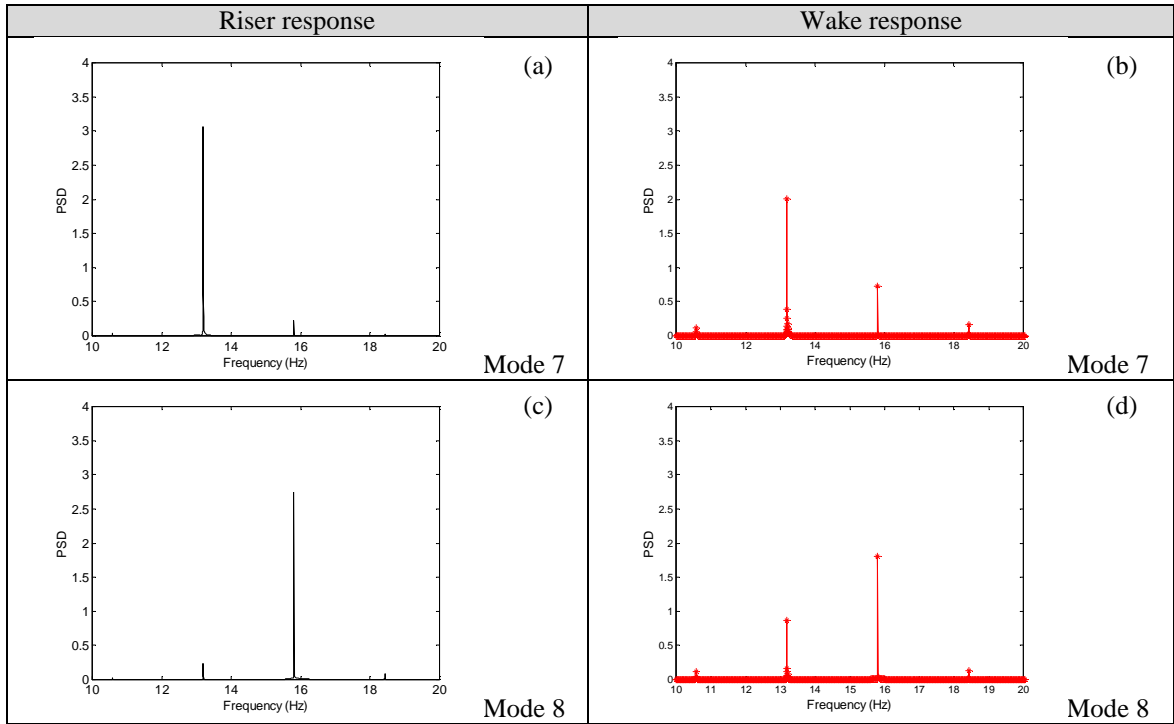


Figure 11

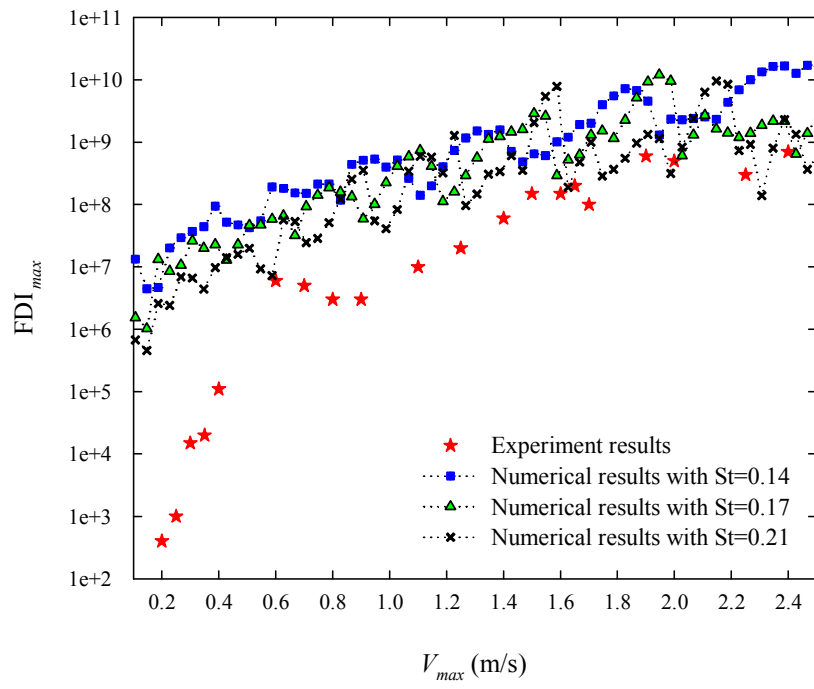


Figure 12

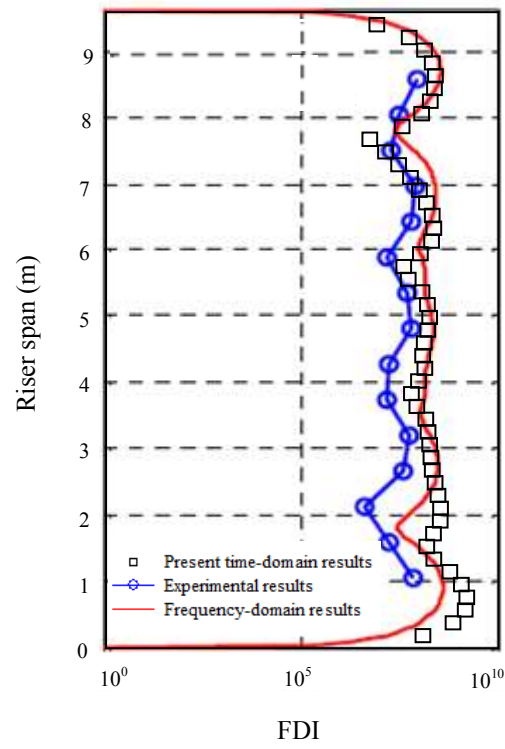


Figure 13